DESY 98-203
December 1998

ISSN 0418-9833

# Probing anomalous boson couplings via "neutrino counting" process

A.A. Likhoded[a)], O.P.Yushchenko[b)]

[a)] *Branch of the Institute for Nuclear Physics, Protvino, 142284 Russia*
E-mail: likhoded@mx.ihep.su

[b)] *Institute for High Energy Physics, Protvino, 142284 Russia.*
E-mail: yushchenko@mx.ihep.su

**Abstract**

The $e^+e^- \to \nu\bar{\nu}\gamma$ process, which is known as "neutrino counting" process, is used to confine three-bosom anomalous $WW\gamma$ couplings. The effective model, in which the interactions responsible for the breaking of electroweak symmetry are strongly coupled, is considered. The bounds on the $WW\gamma$ couplings attainable from the data on the $e^+e^- \to \nu\bar{\nu}\gamma$ reaction are presented. The results for the LEP I, LEP II, and next linear $e^+e^-$-colliders are compared.



## 1 Introduction

The Standard Model of electroweak interactions reveals a remarkable agreement with all precision measurements conducted thus far. However, in spite of its phenomenological success the are several aspects of the Standard Model that still remain unexplained. One of them is the mechanism of the electroweak symmetry breaking. There is a broad class of models in which the interactions responsible for the electroweak symmetry breaking are strongly coupled and which does not contain new particles light enough to be produced at energies below 500 GeV – 1 TeV. It is convenient to describe the phenomenology of such models using the low energy effective Lagrangian approach, in which new physics effects show up themselves as higher dimension operators modifying the couplings of observed particles including "anomalous couplings". Deviations from the self-couplings predicted by the minimal Standard Model have been studied extensively in recent years, and, in particular, they have been discussed in the context of future $e^+e^-$ colliders.

In this paper we study the effect of the lowest dimension operators that lead to anomalous $WW\gamma$-vertex contribution to the $e^+e^- \to \nu\bar{\nu}\gamma$ process at a next 500 GeV $e^+e^-$ collider. This process was discussed previously [1], but we would like to analyze it with respect to its sensitivity to anomalous boson couplings.

This paper is organized as follows. In Section 2 we summarize the effective Lagrangian formalism used to describe the anomalous couplings. In Section 3 we discuss the phenomenology of the $e^+e^- \to \nu\bar{\nu}\gamma$ process in context of the model, present the bounds on anomalous couplings parameterizing triple boson vertex, and compare these bounds with those coming from LEP I and LEP II data. Finally we present our conclusions.

## 2 Anomalous couplings in the context of a strongly-interacting electroweak symmetry breaking sector

For the electroweak symmetry breaking sector we want to describe the case in which there is no light Higgs boson and the low energy particle content is essentially the same as that in the minimal Standard Model providing that Higgs is taken to be very heavy. This model can be written as the ususal standard model, but replacing the scalar sector with the effective Lagrangian [2]:

$$\mathcal{L}^{(2)} = \frac{v^2}{4}\mathrm{Tr}\Big(D^\mu\Sigma^\dagger D_\mu\Sigma\Big)\,.$$

This case was considered at length in the literature [2-6], and we have applied it previously for the $e^+e^- \to W^+W^-$ process [7] and processes with quartic boson interactions [8]. In the model so-called anomalous gauge boson couplings correspond to the contributions from higher dimension operators, which are $SU(2)_L \times U(1)_Y$ gauge invariant. The next to leading order effective Lagrangian that arises in the context of this model and the contributions of this Lagrangian to the anomalous couplings have been discussed in the literature [2-6].

It became common to write down the most general $CP$-invariant $VW^+W^-$ vertex (where $V = Z,\ \gamma$) in the following form [9]:

$$\mathcal{L}_{WWV} = -ie\frac{c_\theta}{s_\theta}g_1^Z\Big(W^\dagger_{\mu\nu}W^\mu - W_{\mu\nu}W^{\mu\,\dagger}\Big)Z^\nu - ieg_1^\gamma\Big(W^\dagger_{\mu\nu}W^\mu - W_{\mu\nu}W^{\mu\,\dagger}\Big)A^\nu$$

$$-ie\frac{c_\theta}{s_\theta}\kappa_Z W^\dagger_\mu W_\nu Z^{\mu\nu} - ie\kappa_\gamma W^\dagger_\mu W_\nu A^{\mu\nu}$$
$$-e\frac{c_\theta}{s_\theta}g_5^Z\epsilon^{\alpha\beta\mu\nu}\Big(W^-_\nu\partial_\alpha W^+_\beta - W^+_\beta\partial_\alpha W^-_\nu\Big)Z_\mu\,. \qquad (1)$$

where $s_\theta = \sin\theta_W$, $c_\theta = \cos\theta_W$.

At the tree level and in unitary gauge the anomalous terms contribute to the process with three-boson and boson-fermion vertices either directly through three-boson $WWV$ vertex, or through renormalization of the $Wf\nu$ and $Zf\bar{f}$ vertices[1].

In the framework of the effective Lagrangian approach and under the assumption that whatever breaks electroweak symmetry has at least an approximate custodial symmetry there are only four operators in the NLO effective Lagrangian that are relevant for the gauge sector (here $v \approx 246$ GeV):

$$\begin{aligned}\mathcal{L}^{(4)} &= \frac{v^2}{\Lambda^2}\Big\{-igL_{9L}\,\mathrm{Tr}\Big(W^{\mu\nu}D_\mu\Sigma D_\nu\Sigma^\dagger\Big) - ig'L_{9R}\,\mathrm{Tr}\Big(B^{\mu\nu}D_\mu\Sigma^\dagger D_\nu\Sigma\Big)\\ &+ gg'L_{10}\,\mathrm{Tr}\Big(\Sigma B^{\mu\nu}\Sigma^\dagger W_{\mu\nu}\Big) + g\hat{\alpha}\epsilon^{\alpha\beta\mu\nu}\mathrm{Tr}\Big(\tau_3\Sigma^\dagger D_\mu\Sigma\Big)\mathrm{Tr}\Big(W_{\alpha\beta}D_\nu\Sigma\Sigma^\dagger\Big)\Big\} \qquad (2)\end{aligned}$$

The effective Lagrangian framework for the case of a strongly interacting symmetry breaking sector allows one to relate the five coupling constants in Eq. (1) with those in Eq. (2) [6,11]:

$$\begin{aligned}g_1^Z &= 1 + \frac{e^2}{c_\theta^2}\Big(\frac{1}{2s_\theta^2}L_{9L} + \frac{1}{(c_\theta^2 - s_\theta^2)}L_{10}\Big)\frac{v^2}{\Lambda^2} + \cdots\,,\\ g_1^\gamma &= 1 + \cdots\,,\\ \kappa_Z &= 1 + e^2\Big(\frac{1}{2s_\theta^2c_\theta^2}\Big(L_{9L}c_\theta^2 - L_{9R}s_\theta^2\Big) + \frac{2}{(c_\theta^2 - s_\theta^2)}L_{10}\Big)\frac{v^2}{\Lambda^2} + \cdots\,, \qquad (3)\\ \kappa_\gamma &= 1 + \frac{e^2}{s_\theta^2}\Big(\frac{L_{9L} + L_{9R}}{2} - L_{10}\Big)\frac{v^2}{\Lambda^2} + \cdots\,,\\ g_5^Z &= \frac{e^2}{s_\theta^2c_\theta^2}\hat{\alpha}\frac{v^2}{\Lambda^2} + \cdots\,.\end{aligned}$$

In Eq. (3) the leading contribution to each anomalous coupling is presented, while $\cdots$ denotes other contributions that arise at higher order ($\mathcal{O}(1/\Lambda^4)$), or at order $\mathcal{O}(1/\Lambda^2)$ with custodial $SU(2)$ breaking. It should be noted here that in contrast to the anomalous couplings set given in [9] we do not have terms which correspond to the usual $\lambda_Z$ and $\lambda_\gamma$, because in the framework of the model discussed they only occur at higher order in $1/\Lambda^2$.

In this paper we will consider the $e^+e^- \to \nu\bar{\nu}\gamma$ process at tree level and work in unitary gauge. From the set of Feynman diagrams contributing to this process (see Fig. 1) one can see that anomalous couplings contribute through $WW\gamma$, $Zf\bar{f}$, and $We\nu_e$ vertices. Adopting that $L_{10}$ is severely constrained by LEP I data we are left with the set of $g_1^\gamma$, $\kappa_\gamma$ anomalous couplings (in terms of Eq. (1)), or with the set of $L_{9L}$, $L_{9R}$ (in terms of Eq. (2)). In the following sections we discuss the phenomenology of these two

[1]However, the contributions from anomalous terms affecting $Wf\nu$ and $Zf\bar{f}$ vertices are proportional to the $L_{10}$ parameter only. It was shown [10] that $L_{10}$ coupling , being proportional to the $\epsilon_3$ parameter measured at LEP I, is tightly constrained, $-1.1 \le L_{10}(M_Z) \le 1.5$, so we will not consider the evolution of this coupling.



constants in the $e^+e^- \to \nu\bar{\nu}\gamma$ process at energy ranges of the LEP and NLC colliders.

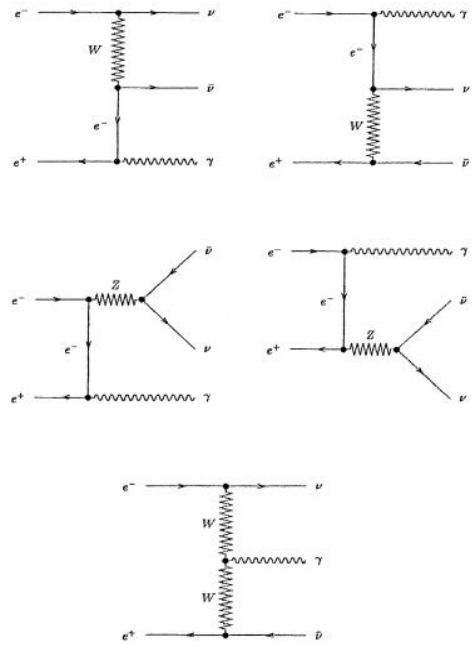


Fig. 1. Diagrams contributing to the process $e^+e^- \to \nu\bar{\nu}\gamma$.

# 3 Phenomenological analysis of the process $e^+e^- \to \nu\bar{\nu}\gamma$

## 3.1 Assumed experimental parameters

In this section we would like to discuss the possible manifestation of anomalous $WW\gamma$ couplings in the process $e^+e^- \to \nu\bar{\nu}\gamma$ at different energy ranges which correspond to LEP I, LEP II, and future linear $e^+e^-$-colliders.

In order to study the anomalous couplings contribution to the process $e^+e^- \to \nu\bar{\nu}\gamma$ at $e^+e^-$-colliders we first need to know some machine and detector parameters and estimate the realistic reconstruction efficiencies and backgrounds. For the process discussed, which has a final state topology of single photon plus missing energy, it should be noted that existing electromagnetic calorimeters allow to detect the energetic photons ($E_\gamma > 3-5$ GeV) with the efficiency $\sim 60\%$. However, about 30% of all photons converts into the $e^+e^-$-pairs on the detector material before entering the EM calorimeter. The reconstruction efficiency of such pairs is about 90% . So, roughly, the expected reconstruction efficiency for single photon is to be about 70%. The detailed study of single photon final state reconstruction with

existing detectors at LEP I [12] and LEP II [13] shows that single photon detection and reconstruction efficiency varies from from 40% to 82% depending on the selection algorithms and criteria. For example, the energy dependence of the reconstruction efficiency was found to be [12]

$$\epsilon(E_\gamma) = A - Ce^{-E_\gamma/B}\,,$$

where $A = 0.70 \pm 0.02$, $B = 2.51 \pm 0.65$, and $C = 0.99 \pm 0.27$, thus, for energetic photons the efficiency value of 70% seems to be quite reasonable and we will use in our analysis.

There are several possibly significant physics backgrounds. First of all, it is $e^+e^- \to e^+e^-\gamma$ radiative Bhabha scattering, in which the photon satisfies the cuts and the final electron and positron escape detection. Other possible sources are the processes $e^+e^- \to \gamma\gamma(\gamma\gamma\gamma)$, in which one (two) photons escape detection. Residual alpha decays and cosmic rays are also contribute. However, it was shown [12] that appropriate choice of data selection algorithm and kinematical cuts allows to suppress the background significantly.

Discussing the phenomenology of the $e^+e^- \to \nu\bar{\nu}\gamma$ for our estimates we accept the following values for energy and integrated luminosity of $e^+e^-$-colliders:

1) for the LEP I collider we will neglect the fact that it performed the scan around $Z^0$-pole and adopt its parameters to be $\sqrt{s} = M_Z = 91.178$ GeV and $\int \mathcal{L}dt = 120$ pb$^{-1}$;

2) For LEP II we assume $\sqrt{s} = 190$ GeV with integrated luminosity of $\int \mathcal{L}dt = 500$ pb$^{-1}$.

3) Detailed simulation [14] for NLC collider, which will be operating at $\sqrt{s} = 500$ GeV and $\int \mathcal{L}dt = 50$ fb$^{-1}$, show that the systematical error will be $\sim$1.4%, and we will use this estimate in our analysis.

For our numerical study we will use the input parameters

$$M_W = 80.37 \text{ GeV}\,, \quad M_Z = 91.187 \text{ GeV}\,, \quad \alpha = 1/128.8$$

## 3.2 Data analysis

Discussing the sensitivity of the $e^+e^- \to \nu\bar{\nu}\gamma$ process to anomalous couplings we will analyze differential cross-sections of the process. We adopt the following philosophy to confine anomalous contributions: one uses the SM predictions as "experimental" data, and considers possible effects due to new physics as small deviations. One then requires agreement between the predictions including new physics and the "experimental" values within expected experimental errors. The parameters representing new physics are, thus, bound by requiring that their effect on the selected observables be smaller than the expected experimental errors.

Using differential cross-sections (angular or energy distributions) we will apply the simplest $\chi^2$-criterion defined as

$$\chi^2 = \sum_i \left(\frac{X_i - Y_i}{\Delta^i_{exp}}\right)^2\,, \tag{4}$$

where, for example, for the case of the angular distribution

$$X_i = \int_{\cos\theta_i}^{\cos\theta_{i+1}} \frac{d\sigma^{SM}}{d\cos\theta} d\cos\theta, \quad Y_i = \int_{\cos\theta_i}^{\cos\theta_{i+1}} \frac{d\sigma^{NEW}}{d\cos\theta} d\cos\theta\,,$$

and $\sigma \equiv \sigma^{SM}$ represents the experimental data, $\sigma^{NEW}$ are the new model predictions, $\Delta^i_{exp}$ are the corresponding experimental errors in bins including statistical and systematical



errors. For binning we subdivide the chosen kinematical range of $\cos\theta$ ($\theta$ is the scattering angle between $e^-$ and $\gamma$) into equal bins. Here:

$$\Delta^i_{exp} = \sigma^{SM}_i \cdot \sqrt{\delta^2_{stat} + \delta^2_{syst}}\,, \quad \delta_{stat} = \frac{1}{\sqrt{N^i_{events}}} = \frac{1}{\sqrt{\epsilon_\gamma \mathcal{L}\sigma^{SM}_i}}$$

## 3.3 Results and discussions

Studying the process $e^+e^- \to \nu\bar{\nu}\gamma$ one should use kinematical cuts, that is necessary for reliable $\gamma$ reconstruction and background suppression

$$\begin{aligned} &\text{I}: \quad 175^o > \theta > 5^o,\ E_\gamma > 10 \text{ GeV},\\ &\text{II}: \quad 178^o > \theta > 2^o,\ E_\gamma > 5 \text{ GeV}, \end{aligned}$$

which correspond to the "pessimistic" (cuts set I) an "optimistic" (cuts set II) variants of final state reconstruction. The total cross-section values for particular collider energy ranges and for two sets of cuts are as follows

| Collider | LEP | LEP II | NLC-500 |
|---|---|---|---|
| $\sqrt{s}$ (GeV) | 91.187 | 190 | 500 |
| $\sigma$ (pb), I | 1.66 | 5.42 | 3.55 |
| $\sigma$ (pb), II | 10.1 | 7.62 | 5.79 |

In Fig. 2 we present the $\sqrt{s}$-dependence of the total cross-section for the cuts set I (however, from now on we will use the set II).

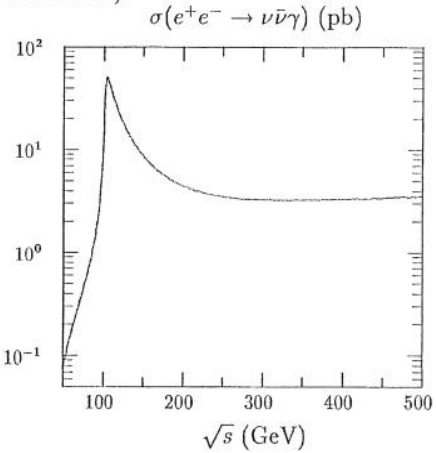


Fig. 2. The $\sqrt{s}$-dependence of the total cross-section for the set of cuts I.

The cross-section has the characteristic resonance peak nearby $Z^0$-pole, that is due to the $s$-channel diagram contributions, and then it becomes flat due to the $t$-channel diagram contributions. It should be noted that at LEP II and NLC energy ranges the cross-section

values are of the same order of magnitude as that one for $e^+e^- \to W^+W^-$, so the resulting bounds coming from both processes could be compatible. From this point of view it is interesting to estimate the sensitivity of the process $e^+e^- \to \nu\bar{\nu}\gamma$ to anomalous couplings at energies of the LEP I, LEP II, and NLC colliders.

It should be noted that anomalous couplings contribute to the process $e^+e^- \to \nu\bar{\nu}\gamma$ only through $WW\gamma$ vertex, and according to Eqs. (1) and (3), the observables depend only on the combination $(L_{9L} + L_{9R})$ and they are not affected by $\hat{\alpha}$-coupling parameterizing $WWZ$-vertex.

In Fig. 3 for demonstration purposes we present the dependence of the relative deviation $(\sigma^{NEW} - \sigma^{SM})/\sigma^{SM}$ for two values of $(L_{9L} + L_{9R})$ (curve 1 corresponds to the case of $(L_{9L} + L_{9R}) = 10$, while curve 2 corresponds to $(L_{9L} + L_{9R}) = -10$, where $\sigma^{NEW}$ is a new model predictions, and $\sigma^{SM}$ corresponds to the SM case.

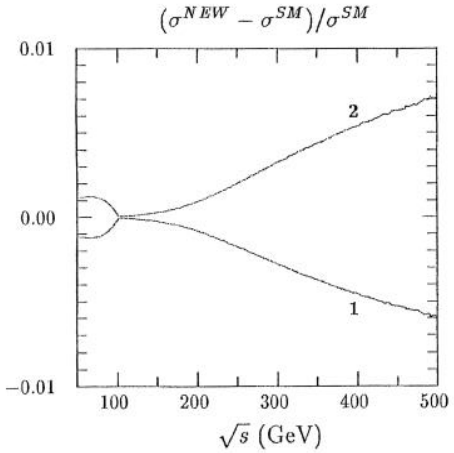


Fig. 3. The $\sqrt{s}$-dependence of the $(\sigma^{NEW} - \sigma^{SM})/\sigma^{SM}$ for the cases of $L_{9L} + L_{9R} = 10$ (curve 1) and $L_{9L} + L_{9R} = -10$ (curve 2).

These curves, in fact, characterize the sensitivity of the total cross-section to anomalous term contributions. From this figure one can see that the relative deviation value is small in the region of the $Z^0$-pole and grows with the energy increase. Hence, one should expect the maximal process sensitivity at higher energies, while at LEP I and LEP II energy regions it is much smaller.

Angular distribution for the process, shown in Fig. 4, is strongly peaked for large $|\cos\theta|$ values. In Fig. 5, where the relative deviation of angle distribution is presented for energies of LEP I, LEP II, and NLC, one can see that the absolute value of this deviation decreases with the $\cos\theta$ increase, so in each of cases it would be useful to impose some angle cuts, $|\cos\theta| \le c_i < 1$, which could suppress the contribution from SM terms and enhance relative contributions of anomalous terms.



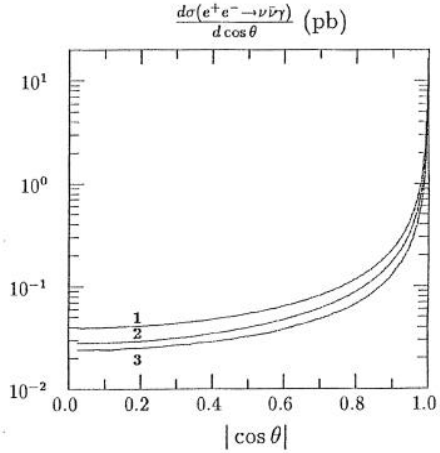


Fig. 4. The angular distribution of the process $e^+e^- \to \nu\bar{\nu}\gamma$ for LEP I (curve 1), LEP II (curve 2), and NLC (curve 3) energies.

To estimate appropriate cut values we analyze the angular dependence of the so-called "statistical significance" defined as

$$S = \frac{|\sigma^{NEW} - \sigma^{SM}|}{\sqrt{\sigma^{SM}}}\sqrt{\mathcal{L}}\,, \tag{5}$$

where $\mathcal{L}$ is the integrated luminosity of the corresponding collider. In Fig. 6 we present the dependence of the $S/\sqrt{\mathcal{L}}$ value on the scattering angle cut for $(L_{9L} + L_{9R}) = 10$ and $(L_{9L} + L_{9R}) = -10$. We found that variation of $(L_{9L} + L_{9R})$ leads to the overall normalization of curves only and does not shift the location of maximums, and one can estimate the corresponding optimal cuts:

| | |
|---|---|
| LEP I | $\lvert\cos\theta\rvert \le 0.891$ |
| LEP II | $\lvert\cos\theta\rvert \le 0.819$ |
| NLC | $\lvert\cos\theta\rvert \le 0.766$ |

These angle cuts we will use in further analysis of the differential cross-section. Studying the angular distributions and using criterion of Eq. (4) to put bounds on anomalous $L_{9L}$, $L_{9R}$ parameters we found that due to the low statistics for the process the best bounds on anomalous couplings can be attained by dividing the $\cos\theta$ interval into 4 equal bins.

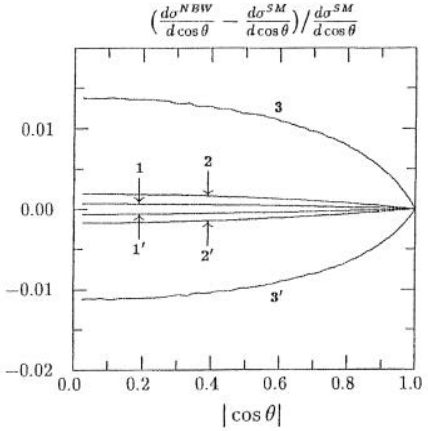


Fig. 5. The $\cos\theta$-dependence of the relative deviation of the differential cross-section for LEP I (curve 1), LEP II (curve 2), and NLC (curve 3) energies for $L_{9L} + L_{9R} = 10$. The curves 1′, 2′, and 3′ correspond to the case of $L_{9L} + L_{9R} = -10$.

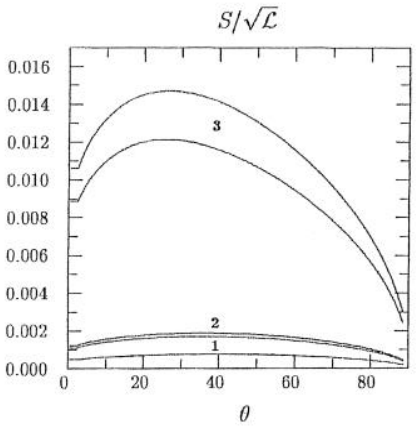


Fig. 6. The dependence of the normalized statistical significance on the angular cut value for LEP I (pair of curves 1), LEP II (pair of curves 2), and NLC (pair of curves 3). For each of cases the upper (lower) curve corresponds to $L_{9L} + L_{9R} = 10$ $(-10)$.

In Fig. 7 we present the resulting allowed regions for $(L_{9L} + L_{9R})$ combination with 95% C.L. coming from the angular distribution analysis for the case of LEP II (the area within dashed lines) and NLC (the area within solid lines) and using $\Lambda = 2$ TeV. The bounds corresponding to the LEP I case are much weaker and can not be presented in this scale. As one could expect the resulting domain for $L_{9L}$, $L_{9R}$ parameters is an infinite band oriented along the straight line $L_{9L} = -L_{9R}$.

However, these bounds can be improved if one considers other possible observable, $d\sigma/dE_\gamma$. In Fig. 8 we present the dependence of the $d\sigma/dE_\gamma$ on the photon energy for the cases of LEP I, LEP II, and NLC. While for the case of LEP I the differential cross-section decreases with the energy of $\gamma$, for the LEP II and NLC cases it has more sharp behaviour, because of the presence of resonance peaks, which are due to the situation when $\nu\bar{\nu}$-pair has invariant mass close to $M_Z$. If one looks onto the behaviour of the relative deviation of $E_\gamma$-dependence shown in Fig. 9, one can see that in contrast to the case of angular distribution it reveals the nontrivial behaviour, and we found that the analysis of statistical significance function (5) does not indicate any reasonable cuts on $E_\gamma$, which could improve the differential cross-section sensitivity to anomalous contributions. Thus, studying the $d\sigma/dE_\gamma$ distributions we will use whole kinematical region for $E_\gamma$. In Fig. 10 we present the allowed regions (95% C.L. and $\Lambda = 2$ TeV) for $(L_{9L},\ L_{9R})$ parameters resulting from the data on the energy distribution for the cases of LEP I (the area bound by short-dashed lines), LEP II (the area bound by long-dashed lines), and NLC (the area bound by solid lines). In each of the cases



these bounds are more strict than those coming from the analysis of the angular distribution.

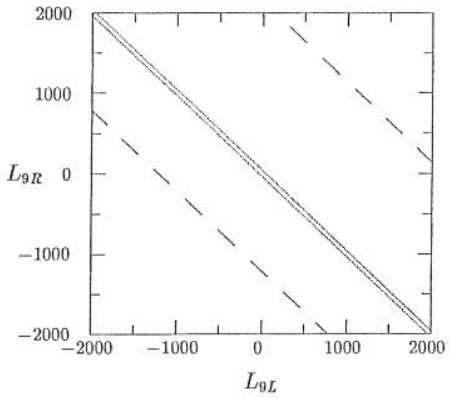


Fig. 7. Allowed regions (95% C.L.) for $L_{9L}$, $L_{9R}$ parameters for LEP II (area bound by dashed lines) and NLC (area bound by solid lines) from the angular distribution.

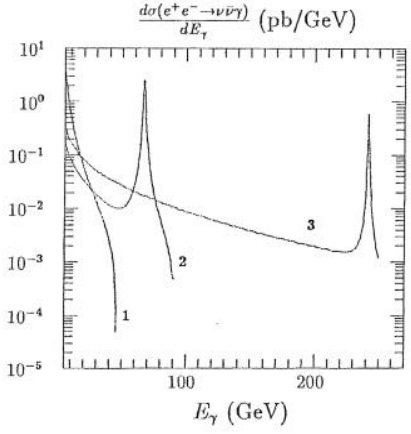


Fig. 8. Differential cross-section $d\sigma/dE_\gamma$ as a function of the photon energy. The notation for the curves is identical to that in Fig. 4.

For example, in Fig. 11 we present the comparison of the bounds from the energy (solid lines) and angular (dashed lines) distributions for the case of NLC. One can see that bounds from the energy distribution seems to be preferable. So, for each case (LEP I, LEP II, and NLC) we will refer to them as final bounds on the $L_{9L}$, $L_{9R}$ couplings. The summary for the bounds, which one can derive from the data on the $e^+e^- \to \nu\bar{\nu}\gamma$ process for LEP I, LEP II and NLC energy regions, is as follows ($\Lambda = 2$ TeV):

$$\begin{aligned} \text{LEP I:} \quad & -3200 \le L_{9L} + L_{9R} \le 3750, \\ \text{LEP II:} \quad & -1000 \le L_{9L} + L_{9R} \le 1500, \\ \text{NLC-500:} \quad & -26 \le L_{9L} + L_{9R} \le 28. \end{aligned}$$

Of course, it is interesting to compare these bounds with those coming from other different processes at LEP I, LEP II and NLC. It was shown [10] that precision measurements of $Z$ partial widths imply:

$$\begin{aligned} -28 \le\ & L_{9L} \le 27\,, \\ -100 \le\ & L_{9R} \le 190\,. \end{aligned} \tag{6}$$

Expected bounds from LEP II coming from data on the process $e^+e^- \to W^+W^-$ [15]:

$$\begin{aligned} -41 \le\ & L_{9L} \le 26\,, \\ -100 \le\ & L_{9R} \le 330\,. \end{aligned} \tag{7}$$

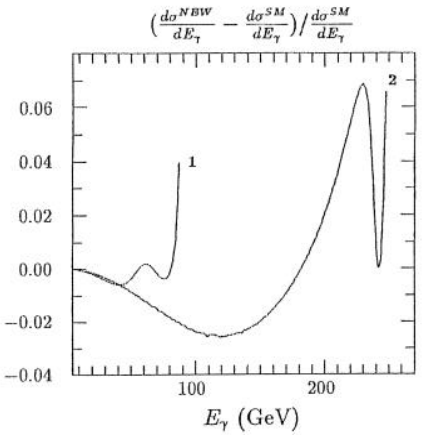


Fig. 9. Relative deviation of the energy distribution for LEP II (curve 1) and NLC (curve 2) at $L_{9L} + L_{9R} = 10$.

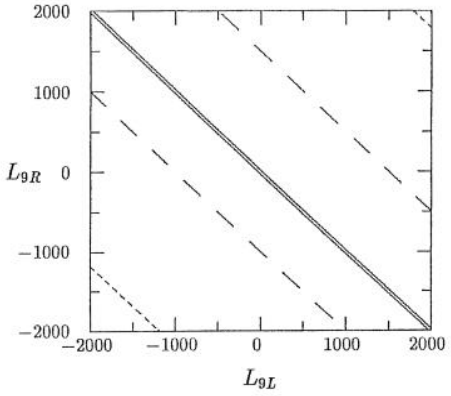


Fig. 10. Allowed regions (95% C.L.) for ($L_{9L}$, $L_{9R}$) from the energy distribution for LEP I (short-dashed lines), LEP II (long-dashed lines), and NLC (solid lines).

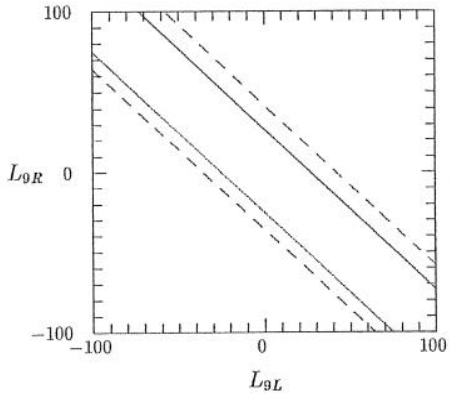


Fig. 11. Allowed regions (95% C.L.) for NLC from the energy (solid lines) and angular (dashed lines) distributions.

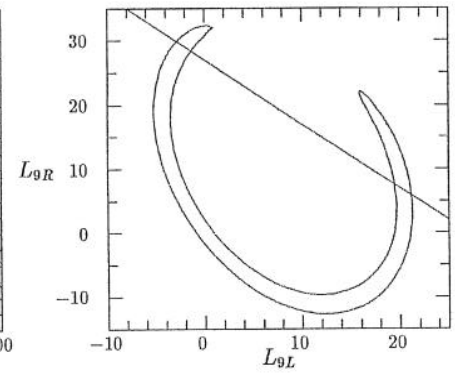


Fig. 12. Allowed regions (95% C.L.) for ($L_{9L}$, $L_{9R}$) from the processes $e^+e^- \to \nu\bar{\nu}\gamma$ (area below straight line) and $e^+e^- \to W^+W^-$ (domain inside curled contour).



The 500-GeV $e^+e^-$-machine with the integrated luminosity of 50 fb$^{-1}$ and unpolarized beams can place the following bounds [7] from the $e^+e^- \to W^+W^-$ process:

$$\begin{aligned} -5 \leq\ & L_{9L} \leq 21\,, \\ -13 \leq\ & L_{9R} \leq 33\,. \end{aligned} \tag{8}$$

So, comparing bounds (6), (7) and (8) with those coming from $e^+e^- \to \nu\bar{\nu}\gamma$ process one finds that this process can not provide any improvement of the bounds from other sources for LEP I and LEP II energies. However, for NLC energies it could be used to put additional constraints on $L_{9L}$, $L_{9R}$ parameters. One can see this effect on Fig. 12, where we compare the NLC bounds from the process under study (allowed region is the area below the straight line) and from the $e^+e^- \to W^+W^-$ data (allowed region is the domain within curled contour). One can see that the $e^+e^- \to \nu\bar{\nu}\gamma$ data allow to exclude some part of the allowed region. In this sense, the bounds coming from both processes at NLC can be considered as complimentary.

## Conclusion

If the electroweak symmetry sector is strongly coupled and no light Higgs will be found at energies below 1 TeV, one could expect the deviation of the boson coupling constants from the SM predictions. In the framework of the model of such type, where anomalous boson interactions are parameterized in terms of several coupling constants, we show that the process $e^+e^- \to \nu\bar{\nu}\gamma$ could be used at an 500 GeV $e^+e^-$-machine to confine the anomalous boson couplings $L_{9L}$, $L_{9R}$ at the level of

$$-26\left(\frac{\Lambda}{2\ \mathrm{TeV}}\right)^2 \leq L_{9L} + L_{9R} \leq 28\left(\frac{\Lambda}{2\ \mathrm{TeV}}\right)^2\,,$$

and these bounds are complimentary to those coming from $e^+e^- \to W^+W^-$ process.

## Acknowledgments

One of authors, A.A.L., would like to express his gratitude to Prof. A. Wagner and members of the DESY Theory Group for kind hospitality during his visit to DESY. The authors would like to thank Prof F. Schrempp for reading this manuscript and making valuable remarks. This work was supported, in part, by RBFR grants 96-02-18216 and 96-15-96575. A.A.L. cordially thanks A.M. Czermak for stimulating discussions.

## References


[1] Ma E., Okada J., *Phys. Rev Lett.* **41** (1978), 287;
Gaemers K.J.F., Gastmans R., and Renard F.M., *Phys. Rev.* **D19** (1979), 1605.

[2] Appelquist T., Bernard C., *Phys. Rev.* **D22** (1980), 200;
Longhitano A., *Nucl. Phys.* **B188** (1981), 118.

[3] Holdom B., *Phys. Lett.* **B258** (1991), 156.

[4] Falk A., Luke M., Simmons E., *Nucl. Phys.* **B365** (1991), 523.

[5] Bagger J., Dawson S., Valencia G., *Nucl. Phys.* **B399** (1993), 364.

[6] Appelquist T., Wu G.-H., *Phys. Rev.* **D48** (1993), 3235.

[7] Likhoded A.A., Han T., Valencia G., *Phys. Rev.* **D53** (1996), 4811.

[8] Dawson S., Likhoded A.A., Valencia G., **hep-ph/96-10299** (1996).

[9] Hagiwara K. et al., *Nucl. Phys.* **B282** (1987), 253.

[10] Dawson S. and Valencia G., *Nucl. Phys.* **B439** (1995), 3; *Phys. Lett.* **B333** (1994), 207.

[11] Kingman Cheung et al., *Phys. Rev.* **D51** (1995), 5.

[12] Abreu P. et al., DELPHI Collaboration, *Z. Phys.* **C74** (1997), 577, and refs. therein.

[13] Ackerstaff K. et al., OPAL Collaboration, **hep-ex/9801024** (1998), and refs. therein.

[14] Frank M. et al., in Proceedings of the Workshop " $e^+e^-$ collisions at 500 GeV: the physics potential", ed. P.M. Zerwas, 1991, p. 223;
Gounaris G. et al., p. 735, ibid.

[15] Boudjema F., Proceedings of "Physics and Experiments with Linear $e^+e^-$ Colliders" Workshop, ed. by F. A. Harris et al., World Scientific, Singapore, 1993 , p. 713, and refs. therein.